Carbon 136 (2018) 11–20

Contents lists available at ScienceDirect

Carbon

journal homepage: www.elsevier.com/locate/carbon

Quantitative morphological analysis and digital modeling of polydisperse anisotropic carbon foam

Frederick Arand [a, b, *], Jürgen Hesser [b]

[a] Volume Graphics GmbH, Speyerer Str. 4-6, D-69115 Heidelberg, Germany
[b] Experimental Radiation Oncology, Medical Faculty Mannheim, Heidelberg University, Theodor-Kutzer-Ufer 1-3, D-68167 Mannheim, Germany

ARTICLE INFO

Article history:
Received 21 February 2018
Received in revised form
6 April 2018
Accepted 18 April 2018
Available online 24 April 2018

ABSTRACT

Digital models of open cell carbon foam often approximate pore space by a set of overlapping spheres. In this paper, we extend this strategy to overlapping ellipsoids of varying size and anisotropy. A typical application is demonstrated: After a carbon foam sample is digitized with a computed tomography (CT) scanner, pores are analyzed with respect to polydispersity and anisotropy. Digital foam is created in two steps. First, a heuristic bubble growth simulation yields an overlapping ellipsoid packing, representing large pores. Small pores are then added to the remaining material. Finally, sample and digital model are compared by Finite Element (FE) analysis. Our results show that the foam model agrees well with the analyzed sample when considering pore statistics. However, mechanical simulations show differences, with an average effective elastic modulus of 0.341 GPa for the sample, compared to 0.153 GPa for the model. The approach of digital foam allows to assess the potential and limitation of diverse analysis techniques for CT scans of foam and hence gives respective limits. FE simulations help to identify accurateness of digital models.

1. Introduction

Porous structures can be ubiquitously found in nature [1]. In particular, bones are an interesting field of research [2], and show the significant advantage of foam structures compared to homogeneous bulk material, i.e., low weight combined with highly favorable physical properties, for example resistance to mechanical stress.

Industrial foams are inspired by nature and are produced with similar motivation. Aluminum foam is covered extensively by research, often with the help of computed tomography (CT) [3–5]. Morphological analysis, mechanical experiments and Finite Element (FE) simulations are common tools to gain insights in material properties [6,7]. Digital material modeling has been studied more generally for many years, with a large set of applications [8–12].

Because of the seemingly regular and geometrical void space, carbon foams are well suited for digital modeling. Their void space is often approximated by a set of overlapping spheres, which is the consequence of a nearly spherical bubble growth process during production [13,14]. However, according to Beechem et al. [15], anisotropic bubbles are common in the majority of foaming processes.

Sihn and Roy [16] modeled carbon foam based on its microstructure. The authors used tetrahedral unit cells as the basis of a sphere packing, where each unit cell contained ligaments intersecting in a central node. After variation of microstructural properties inside the unit cell and FE analysis, the authors conclude that mechanical bulk moduli of carbon foam can mainly be enhanced by improving transverse and shear properties of the middle section of ligaments, while nodal points only have a small influence on bulk behavior.

Kırca et al. [17] created a computer-aided design (CAD) model of carbon foam. Random positions were used for sphere centers, and previously measured statistics of a foam geometry were used to model sphere radii. The resulting sphere configuration acted as void space of the generated artificial foam. In a final step, the CAD model was analyzed with of a FE software, and mechanical properties were compared to literature.

James et al. [18] developed a sphere placement algorithm based on measurements of the geometry of real foam. The resulting digital foam was qualitatively compared to scanning electron

* Corresponding author. Volume Graphics GmbH, Speyerer Str. 4-6, D-69115 Heidelberg, Germany.
E-mail address: fredi.arand@gmail.com (F. Arand).

https://doi.org/10.1016/j.carbon.2018.04.049
0008-6223/

microscopy (SEM) images.

Dyck and Straatman [19] generated virtual foams using a Discrete Element Method, and designed a bubble contact law based on observations of physical foam production processes. The resulting geometry was then used for computational fluid dynamics simulations.

Similarly to previous works, the aim of this study is to create a digital model which comes as close as possible to a given foam sample. The novelty in this paper lies in a detailed analysis of polydispersity and anisotropy, combined with a digital model that is able to reproduce these two aspects quantitatively. Finally, simulated effective mechanical properties are used to survey effective similarity of sample and model.

2. Methods

In order to analyze the morphological structure of a foam sample, its void space is segmented into pores. The relation between pores and void space is the same as the relation between caves and a cave system. Pore analysis is subdivided into two parts. First, polydispersity, i.e., distribution of pore sizes, is quantified. Second, anisotropy of pores is analyzed. In the subsequent digital model, all pores are modeled as ellipsoids of varying size and anisotropy, where ellipsoid bodies may overlap. Finally, elasto-mechanical simulations are used to calculate effective properties of sample and model foam.

2.1. Polydispersity of sample

Before morphological analysis of the CT data set, volume data is preprocessed. Noise is removed with non local means filtering [20], where denoising parameters are chosen automatically according to [21]. It should be noted that more recent, advanced denoising filters could also be used at this stage [22].

A global threshold for segmentation is chosen to distinguish material from void space. Choosing the threshold is critical: variation of the threshold probably leads to a change in porosity and might even change pore space configuration, for example with respect to connectivity of pores. Interesting suggestions for automatic threshold determination exist, for example in the work of Tenginakai et al. [23]. However, the implementation yielded ambiguous results. Instead, a simple and reproducible approach is taken: First, background and material peaks are identified in the grey value histogram of the data set. Then, the threshold is chosen at the minimum between the identified peaks.

The final preprocessing step makes sure that no free-floating material voxels are present in the data set: If a material voxel is not connected to the boundary of the volume via other material voxels in its 26-neighborhood, then it is erased and becomes void space.

Next, the CT scan is examined with respect to the topology of its void space. Terminology in this work follows the one of pore network algorithms [24,25], and is different to previous publications about virtual carbon foams. *Pores* and *throats* in this article are equivalent to *bubbles* and *pores* in Refs. [17] and [18]. Definitions of pores and throats follow later in the text.

Previous publications argued that void space can be approximated by sphere packings. Distributions of sphere diameters were extracted by visual inspection of 2D SEM [16,18], not quantified in detail [17], or chosen from a normal distribution [19]. In this work, 3D void space is segmented automatically, without prior assumptions about constituting shapes. Morphology analysis is based on the modified maximal ball algorithm (mMBa) [26], which is a recent improvement of the maximal ball algorithm [24,25]. The mMBa partitions void space into pores and throats. A pore is a simply connected sub volume of void space, the latter is also called pore space. Throats are membranes of 1 voxel thickness and lie in between pores. Other, application-dependent definitions of throats exist as well [27]. A visualization of void space partitioning is found in Fig. 1. It shows qualitatively that spheres are a good basis for modeling, but non-spherical pores might yield a more realistic representation of the foam [15].

After automatic segmentation, pores are quantified with respect to pore sizes. Polydispersity is related to (relative) pore volumes V_{pore}, which are obtained by counting voxels inside pores. In order to make pore sizes more conceivable, effective pore radii, r_{eff}, are calculated for each pore, such that

$$V_{\text{pore}} = \frac{4}{3}\pi r_{\text{eff}}^3 \tag{1}$$

For convenience, r_{eff} is shortened to r occasionally. It should be noted that r_{eff} can be calculated for arbitrarily shaped volumes, but serves well as an indicator for order of magnitude, i.e., length scales are more intuitive than volume scales.

2.2. Anisotropy of sample

Anisotropy of pores is measured using principal component analysis: First, the covariance matrix $\mathbf{\Sigma}$ of pore P is calculated from its voxel distribution,

$$\mathbf{\Sigma} = \sum_{\mathbf{x}_i \in} (\mathbf{x}_i - \langle \mathbf{x} \rangle)(\mathbf{x}_i - \langle \mathbf{x} \rangle)^T \tag{2}$$

where voxel position $\mathbf{x}_i$ is a column vector, $\langle \mathbf{x} \rangle$ is the average voxel position inside P, and $(\cdot)(\cdot)^T$ is the dyadic product of two vectors. Then, principal axis can be extracted from $\mathbf{\Sigma}$ using eigenvalue decomposition:

$$\mathbf{\Sigma} = \boldsymbol{V}\boldsymbol{\Lambda}\boldsymbol{V}^T \tag{3}$$

with orthonormal eigenvectors

$$\boldsymbol{V} = [\mathbf{v}_1, \mathbf{v}_2, \mathbf{v}_3] \tag{4}$$

and eigenvalues

$$\boldsymbol{\Lambda} = \text{diag}(\lambda_1, \lambda_2, \lambda_3) \tag{5}$$

Finally, can be approximated by an ellipsoid $\mathscr{E}$ [28], where axis

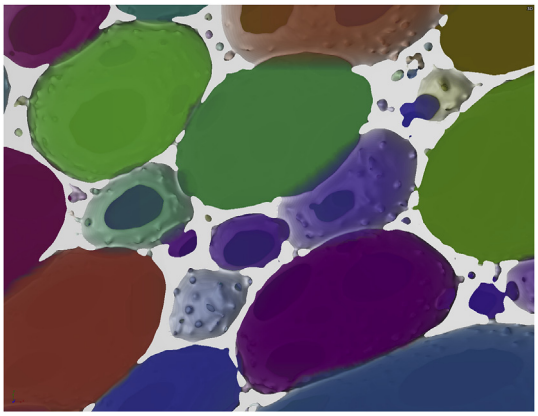

Fig. 1. Automatic partition of void space. Material is colored white, pores are rendered as fog with random colors. Throats are membranes between pores and are colored grey. Renderings in this work are produced with the software VGStudio MAX 3.1. (A colour version of this figure can be viewed online.)